

Supplement of Atmos. Chem. Phys., 19, 11525–11543, 2019
<https://doi.org/10.5194/acp-19-11525-2019-supplement>
© Author(s) 2019. This work is distributed under
the Creative Commons Attribution 4.0 License.



Supplement of

Vertical profile observations of water vapor deuterium excess in the lower troposphere

Olivia E. Salmon et al.

Correspondence to: Lisa R. Welp (lwelp@purdue.edu)

The copyright of individual parts of the supplement might differ from the CC BY 4.0 License.

Supplemental Information Sections

Section S1. Comparison of Los Gatos Research (LGR) and Picarro H₂O_v mole fraction measurements

Section S2. Water vapor concentration-dependence calibration

Section S3. Water vapor δD , $\delta^{18}O$, and d-excess error propagation

Section S4. Equilibrium fractionation factor method comparison

Section S5. Case study weather maps

Section S6. Fractionation of water vapor in ice supersaturated conditions

Section S7. Indianapolis International Airport (KIND) temperature and dewpoint profiles preceding and during DBL observations

Section S1. Comparison of LGR and Picarro H₂O_v mole fraction

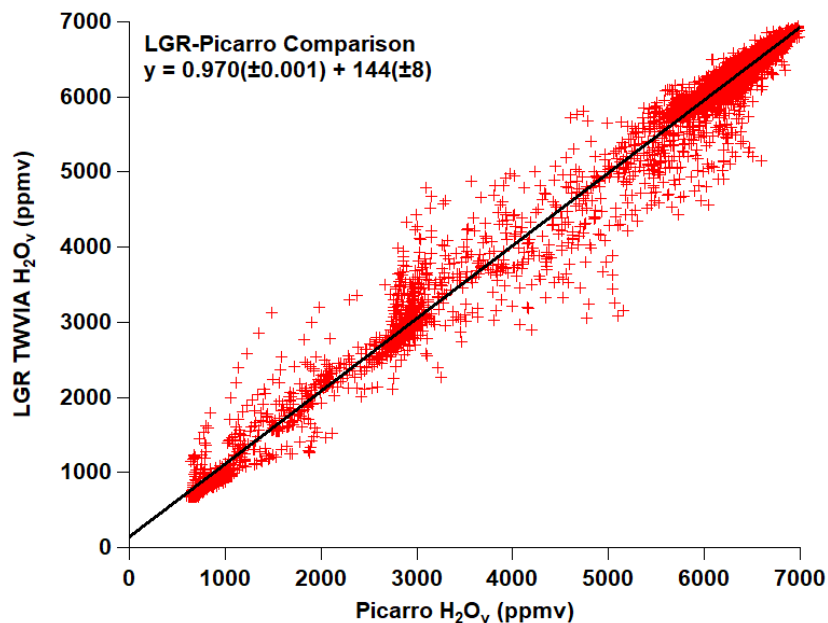


Figure S1: Concentration-dependence calibrated H₂O_v mole fractions from the Los Gatos Research (LGR) Triple Water Vapor Isotope Analyzer (TWVIA) and the Picarro cavity ringdown spectrometer during the entire flight conducted on 6 March 2016 (CLR). The purpose of this plot is for measurement comparison only; it is not used to calibrate either H₂O_v data set.

Section S2. Water vapor concentration-dependence calibration

A Los Gatos Research (LGR) Water Vapor Isotope Standard Source (WVISS; model: 908-0004-9003) equipped with a secondary dry air mixing chamber for extended range operation was used to characterize the LGR Triple Water Vapor Isotope Analyzer's (TWVIA; model: 911-0034) non-linear response to water vapor (H_2O_v) concentration (Rambo et al., 2011). The WVISS samples liquid water with a known isotopic composition from a reservoir. The standard sample is then nebulized using zero (dry) air into a heated chamber (75°C), where it evaporates completely and is further diluted with zero (dry) air with programmable flow rates to output a range of H_2O_v fractions with the same isotopic signature as the liquid standard. Different combinations of nebulizer sizes (flow rates) and standard versus extended range operation were required to span a large range of H_2O_v values. The TWVIA's H_2O_v dependence (while operating in extended range mode, ~ 80 Torr) was evaluated over the range from 550 ppmv – 14,000 ppmv, consistent with range of H_2O_v mole fractions observed during the research flights (Table 1). Free troposphere H_2O_v mole fractions were sometimes less than 550 ppmv, but the lowest H_2O_v mole fraction the WVISS can produce is 500 ppmv. We found that stable flows of H_2O_v mole fractions lower than 550 ppmv were difficult to achieve with the WVISS, so we opt not to report δD and $\delta^{18}\text{O}$ values corresponding to observed H_2O_v mole fractions below 550 ppmv. The δD and $\delta^{18}\text{O}$ values of the H_2O_v isotope standards, which bracket the ranges observed during the research flights (Table 1), are listed in Table S2. The WVISS was programmed to sample each H_2O_v mole fraction for ≥ 20 min. The δD and $\delta^{18}\text{O}$ H_2O_v dependence calibration curves were constructed from the average δD and $\delta^{18}\text{O}$ values reported during the last 200 s of each calibration period to remove any influence of transition instability caused by water moving onto and off of the walls of the system during the calibration H_2O_v step changes. The $\delta^{18}\text{O}$ and δD H_2O_v dependence curves shown in Fig. S2.1 and Fig. S2.2, respectively, were fit using the locally weighted polynomial regression “locpoly” function from R's “locfit” package (Bailey et al., 2015). A 100 ppmv sliding window was used for the local polynomial regression fitting over the range from 550 ppmv – 14,000 ppmv H_2O_v .

Table S2: Calibration standards

Standard*	δD (‰)	$\delta^{18}\text{O}$ (‰)	d-excess (‰)
Purdue tap water	-39.9	-8.7	29.7
Boulder tap water	-117.3	-15.4	5.9
USGS-46	-235.8	-29.8	2.6
South Pole Glacier Water	-434.5	-54.3	-0.1
Custom Light Blend [†]	-573.7	-76.2	36.1

*Standard values are reported relative to the VSMOW-SLAP scale

[†]The Custom Light Blend is a mixture of Purdue tap water, Sigma Aldrich deuterium depleted water (≤ 1 ppm HDO), and Isotec 95% H_2^{18}O (^{18}O -enriched) to achieve a depleted isotopic signature that brackets the most depleted research flight observations of δD and $\delta^{18}\text{O}$ that also has a realistic d-excess signature. Because the Custom Light Blend is isotopically more depleted than our standards, known amounts of the Custom Light Blend and Purdue tap water were combined to make three mixtures, which were analysed using an LGR liquid water isotope analyser (T-LWIA-45-EP; model: 912-0050-0001) to determine the Custom Light Blend's isotopic signature.

The TWVIA's H_2O_v dependence curve was reproducible over all $\delta^{18}\text{O}$ isotope standard signatures considered (Table S2). The $\delta\text{D}-\text{H}_2\text{O}_v$ dependence curve was reproducible for the three relatively enriched isotope standards, more enriched than -235.8‰ in Table S2, but was not always reproducible using the most depleted standards (South Pole Glacier and Custom Light Blend) over the H_2O_v range of ~ 3000 ppmv to ~ 8000 ppmv (Fig. S2.1a and Fig. S2.2a). At H_2O_v mole fractions outside that range, the calibration curve remained reproducible. The cause of the 3000 ppmv – 8000 ppmv irreproducibility of the $\delta\text{D}-\text{H}_2\text{O}_v$ dependence curve associated with very depleted δD values remains unknown, perhaps small leaks in the experimental setup, uncertainty associated with curve fitting, or instrument biases or lower instrument precision for very depleted δD values. To our knowledge this behaviour has not been described in the literature. However, δD values consistent with the two most depleted standards (Table S2) were only observed in the free troposphere. These correspond to low H_2O_v mole fractions (<1000 ppmv) and were outside of the irreproducible window of H_2O_v values. Therefore, it was not consequential to actual flight observations in this experiment. We note that there also appears to be large variability in the TWVIA-reported δD values <1000 ppmv H_2O_v for the two depleted standards, but there is also relatively larger variability in this H_2O_v range for the enriched standards as well. To avoid biases resulting from the depleted δD irreproducibility, the δD water vapor dependence curve is defined using calibration data from the three relatively enriched standards. However, δD calibration data from each of the five standards is used to define uncertainties (see below in Section S3).

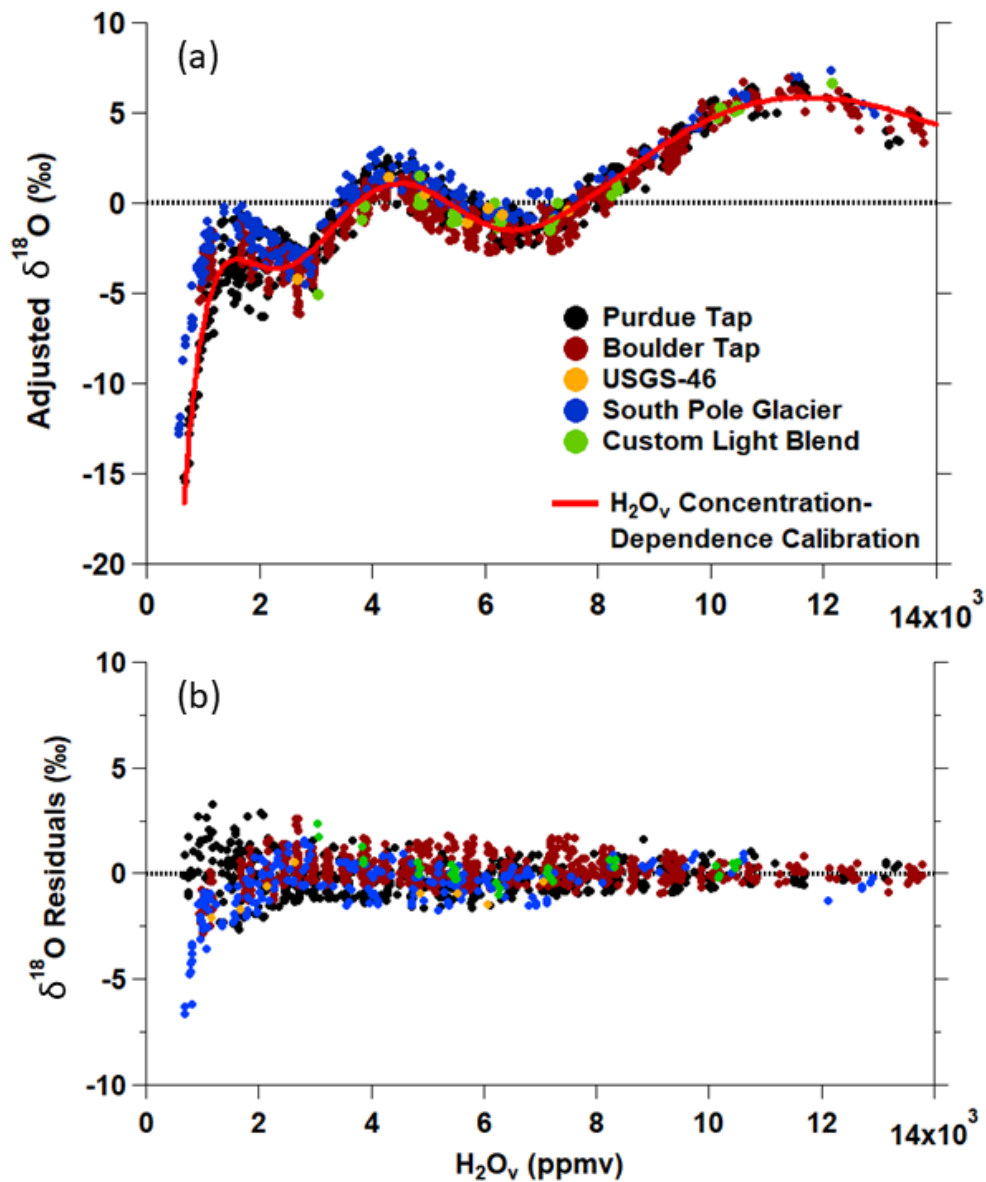


Figure S2.1: $\delta^{18}O$ - H_2O_v dependence (a) calibration curve and (b) residuals. The true $\delta^{18}O$ signature of each standard (Table S2) has been subtracted from the TWVIA measurements to give the “adjusted” $\delta^{18}O$ signature in (a). Residuals are calculated by subtracting points along the H_2O_v dependence curve from the measured calibration data points.

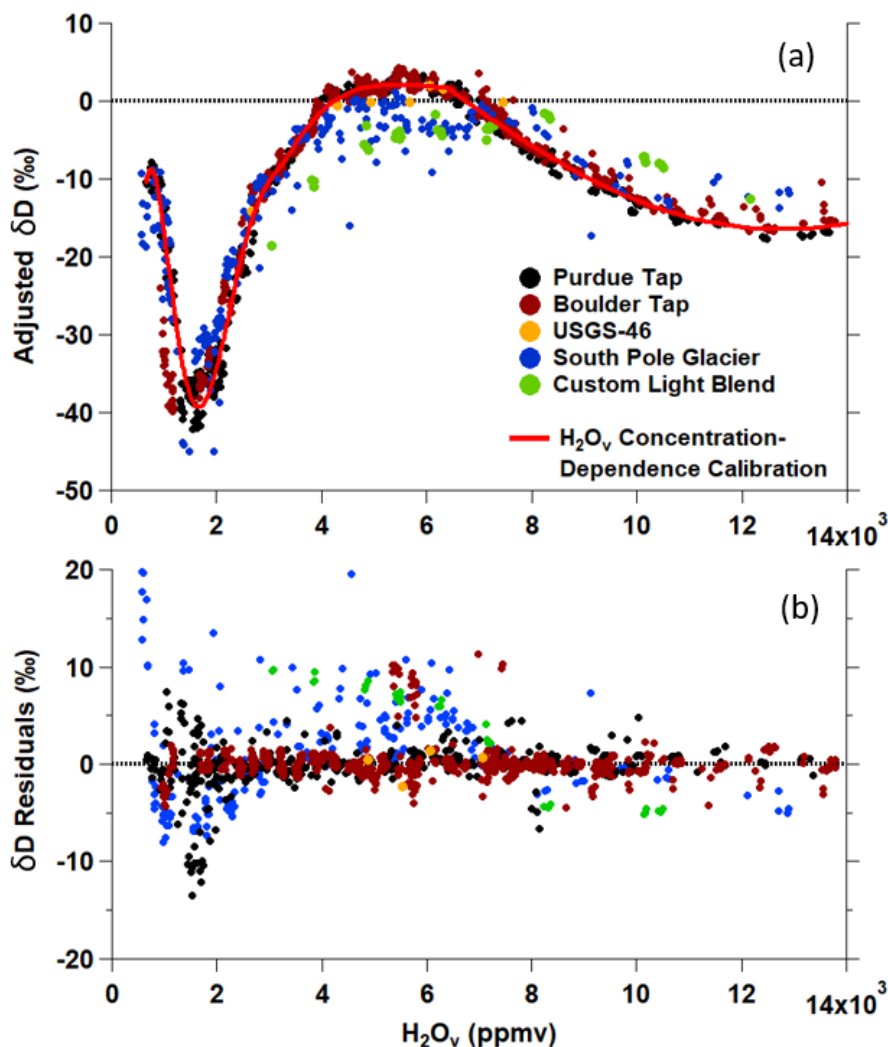


Figure S2.2: δD - H_2O_v dependence (a) calibration curve and (b) residuals. The true δD signature of each standard (Table S2) has been subtracted from the measurements to give the “adjusted” δD signature in (a). Residuals are calculated by subtracting points along the H_2O_v dependence curve from the measured calibration data points.

The linear regressions of the isotope standards’ H_2O_v concentration-dependence corrected δ values versus true gas phase isotopic signature for $\delta^{18}O$ and δD have slopes near unity and intercepts near zero (Fig. S2.3). $\delta^{18}O$ had a slope of $1.009(\pm 0.001)$, a y-intercept of $0.08(\pm 0.03)$, and an R^2 of 0.997254 (Fig. S2.3a). The δD ordinary least squares regression line had a slope of $0.9954(\pm 0.0005)$, a y-intercept of $-0.5(\pm 0.09)$, and an R^2 of 0.99958 (Fig. S2.3b). A VSMOW-SLAP correction was not applied because it would be negligible compared to the uncertainty associated with the concentration-dependence correction and the instrument precision (Section S3).

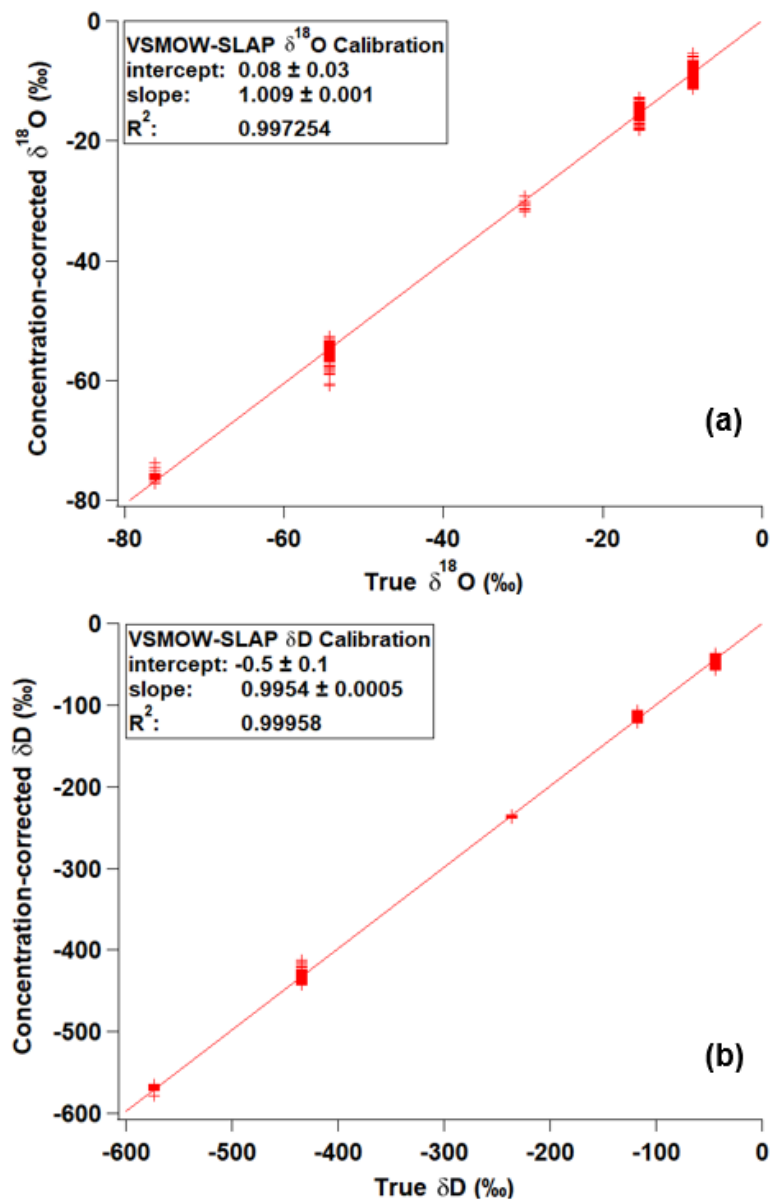


Figure S2.3. VSMOW-SLAP calibration curves for (a) $\delta^{18}\text{O}$ and (b) δD . H_2O_v -concentration-corrected isotopic signatures are plotted against the standard's true isotopic signature. Linear regression fit slopes and intercepts are included in the figure insets.

Section S3. Water vapor δD , $\delta^{18}O$, and d-excess error propagation

Instrument precision:

The TWVIA instrument precision was calculated as the 1σ standard deviation for the last 20 seconds of every calibration period (Section S2). The interval used to smooth the δD , $\delta^{18}O$, and d-excess values reported in this paper is 20 s, which corresponds to the time required for the TWVIA signal to stabilize after a change in the sample's H_2O_v mole fraction or isotopic signature. Power functions were fit to the δD and $\delta^{18}O$ precision values from all the calibrations as a function of H_2O_v mole fraction (Fig. S3). Precision uncertainties for flight measurements were calculated using the measured H_2O_v mole fraction and the power fit functions.

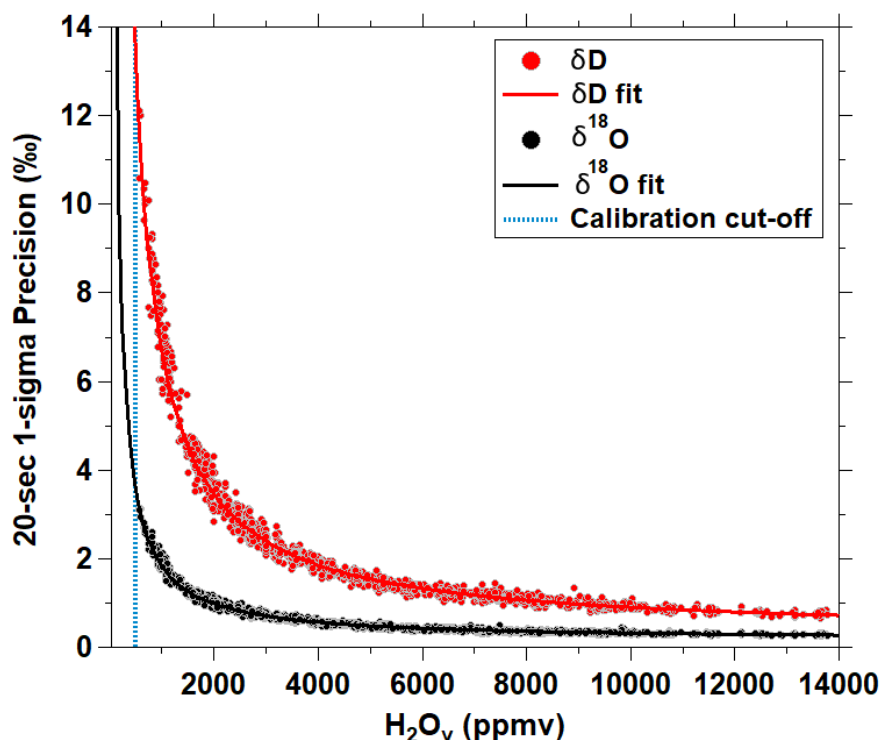


Figure S3: TWVIA $\delta^{18}O$ and δD 20-s instrument precision (1σ) as a function of water vapor (H_2O_v) mole fraction for all calibration data.

H_2O_v dependence calibration uncertainty:

The uncertainty associated with the TWVIA δD - and $\delta^{18}O$ - H_2O_v dependence corrections is determined from the calibration residuals shown in Fig. S2.1b and Fig. S2.2b. We note that the calibration residuals do include a small instrument precision component, as the calibration values are the average of 200 s sampling periods. The absolute value of the δD and $\delta^{18}O$ residuals from all five reference waters tested were filtered into bins defined by 100 ppmv H_2O_v mole fraction increments. Averages of the absolute δD and $\delta^{18}O$ residuals were calculated for each bin. For relatively dry conditions (i.e. below 3500

ppmv H₂O_v), the bin-averaged calibration residuals increase as H₂O_v mole fractions decrease. A best-fit linear regression was determined for the bin-averaged residuals as a function of H₂O_v mole fraction (from 550 – 3500 ppmv for δD and 550 – 3700 ppmv for δ¹⁸O). Bin-averaged residuals were relatively constant for H₂O_v mole fractions greater than 3500 ppmv for δD and 3700 ppmv for δ¹⁸O. Average H₂O_v dependence calibration uncertainties of 1.8‰ for δD and 0.9‰ for δ¹⁸O were calculated from the bin-averaged residuals from 3500 – 14000 ppmv for δD and 3700 – 14000 ppmv for δ¹⁸O. Higher uncertainties in the δ values at low H₂O_v mole fractions is not surprising, as the manufacturer suggests the TWVIA be used for sampling air ranging from 4,000 – 60,000 ppmv H₂O_v.

Total uncertainty:

Total δD and δ¹⁸O uncertainty is calculated by propagating the error resulting from instrument precision, $S_{precision}$, and from the H₂O_v concentration-dependence calibration, $S_{calibration}$, as in eq. (S3.1):

$$S_{total} = \sqrt{S_{precision}^2 + S_{calibration}^2}. \quad (S3.1)$$

The total d-excess uncertainty is determined according to eq. (S3.2):

$$S_{total,d-excess} = \sqrt{S_{total,\delta D}^2 + 8 \times (S_{total,\delta^{18}O}^2)}, \quad (S3.2)$$

where $S_{total,\delta D}$ and $S_{total,\delta^{18}O}$ are the total δD and δ¹⁸O uncertainties (given by eq. (S3.1)). The total uncertainty for δD, δ¹⁸O, and d-excess as functions of H₂O_v mole fraction are presented in Fig. 1.

Section S4. Rayleigh distillation equilibrium fractionation factor method comparison

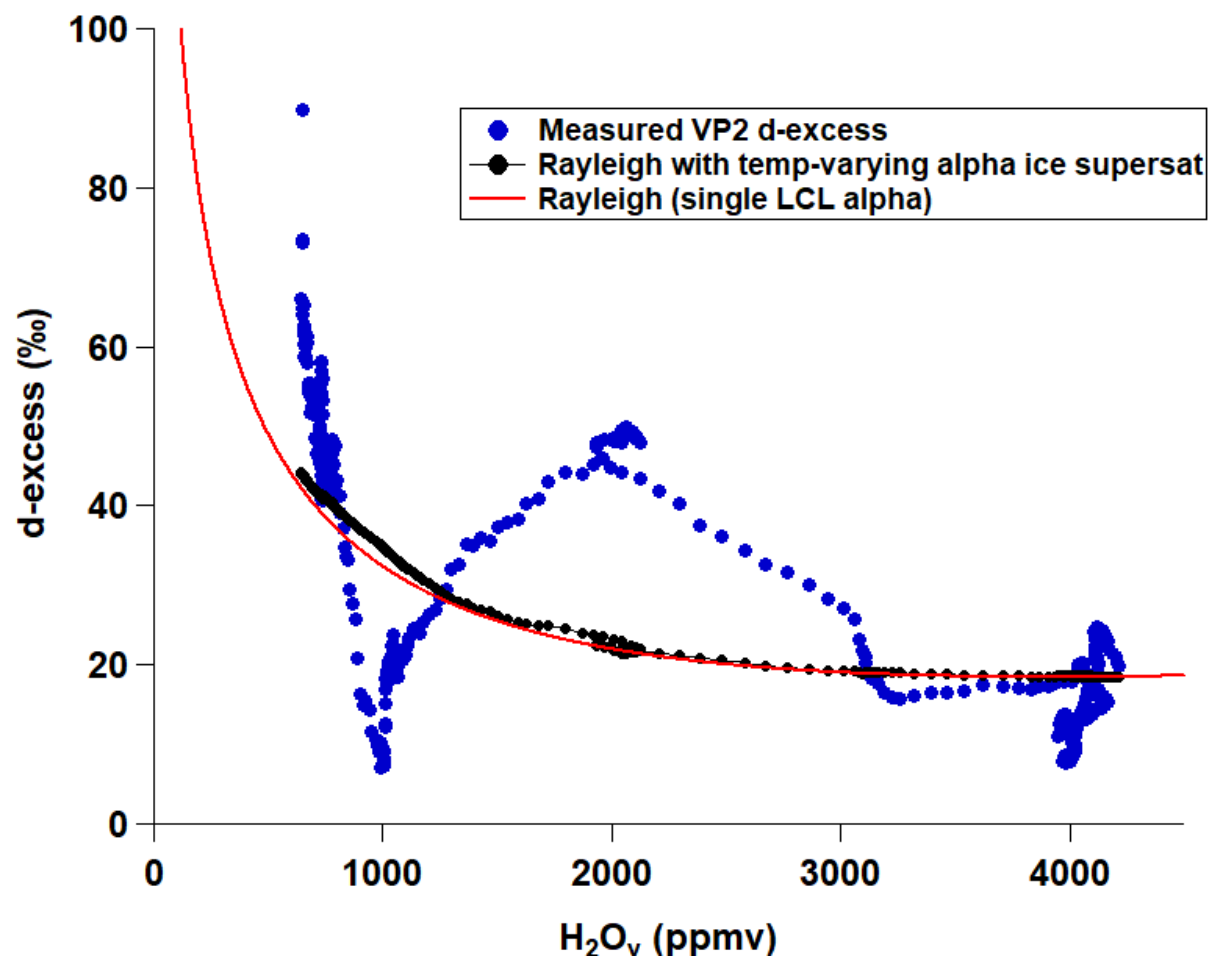


Figure S4. Comparison of Rayleigh distillation curves calculated using a single fractionation factor (α) defined by the temperature at the lifting condensation level (LCL = -6.0°C) and temperature-varying α values. The Rayleigh curve comparison is shown for altitude-varying temperatures, ranging from -0.9°C – 4.1°C , measured along the second vertical profile (VP2) conducted on the stratocumulus cloud (STC) case study.

Section S5. Case study weather maps

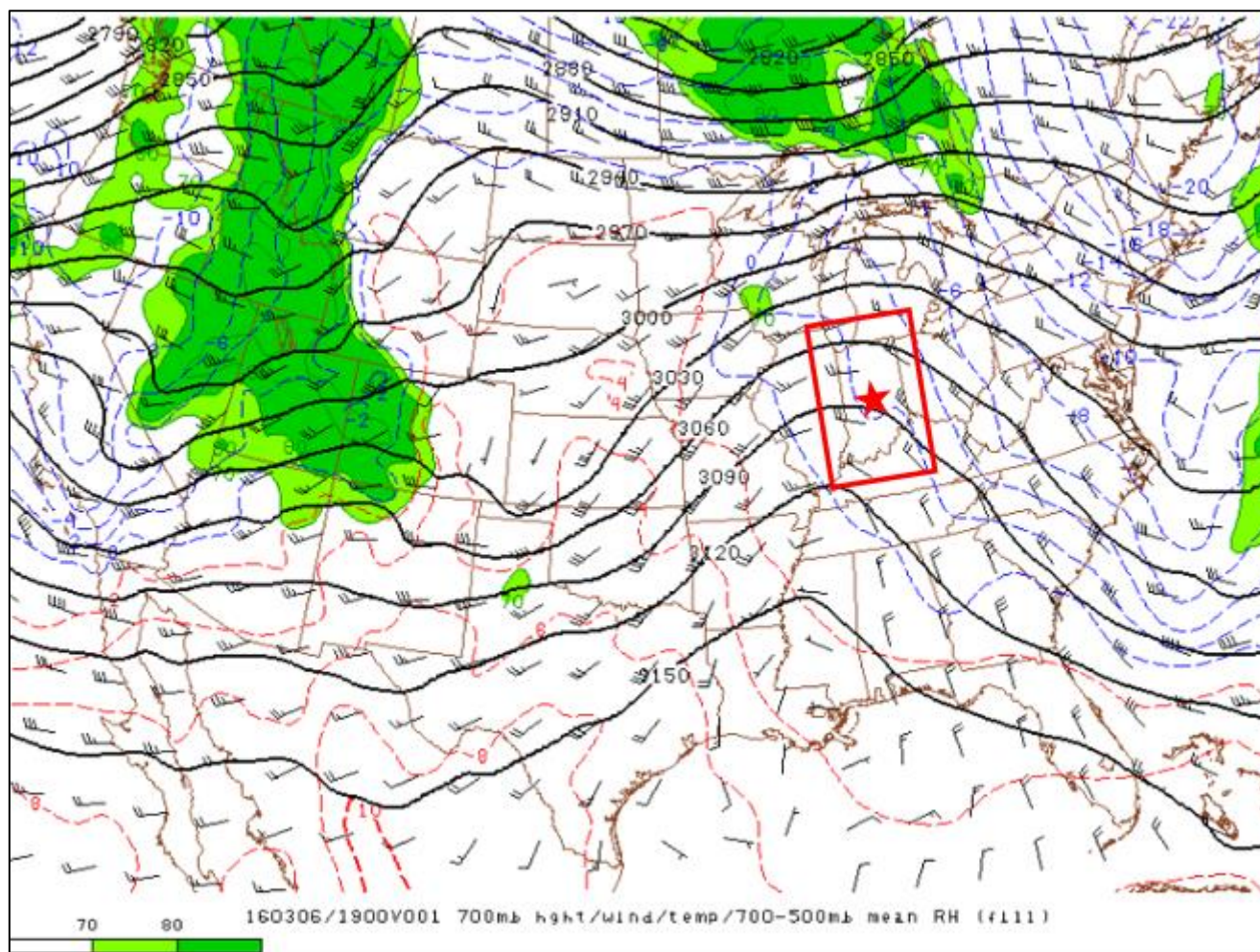


Figure S5.1. Weather map of mid-troposphere (3-5.5 km) relative humidity on the CLR case study day (6 March 2016) at 14:00 local time (EST). Figure S5.1 shows that the mid-troposphere was relatively dry directly upwind of the Indianapolis study site. Indiana is outlined by a red box, and Indianapolis is indicated with a star. This weather map represents atmospheric conditions approximately halfway through the CLR flight. Map source:

https://www.spc.noaa.gov/exper/ma_archive/.

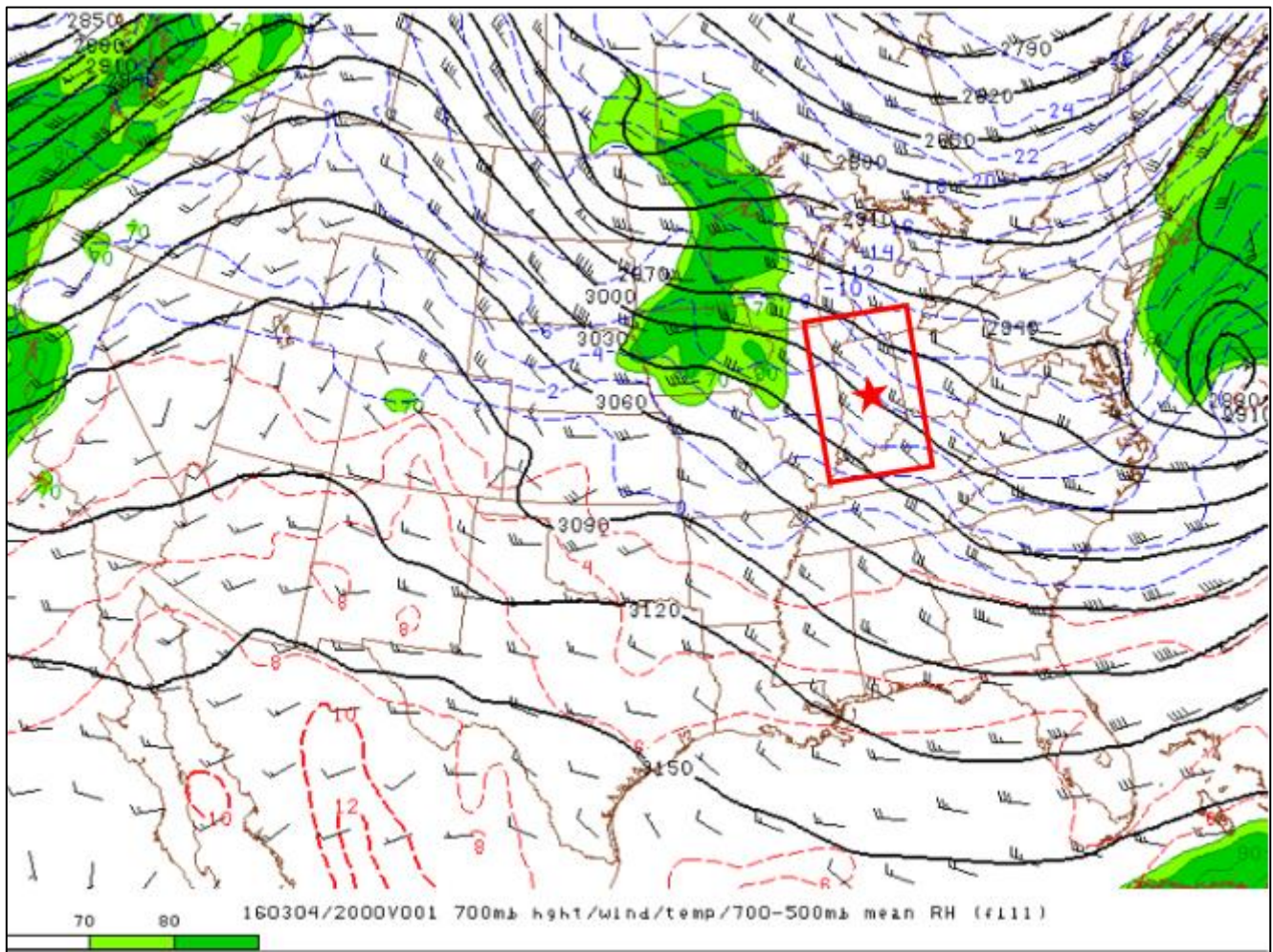


Figure S5.2. Weather map of mid-troposphere (3-5.5 km) relative humidity on the STC case study day (4 March 2016) at 15:00 local time (EST). Figure S5.2 shows an atmosphere of >80% relative humidity (dark green coloring) upwind of the Indianapolis study site. Indiana is outlined by a red box, and Indianapolis is indicated with a star. This weather map represents atmospheric conditions approximately halfway through the STC flight. Map source: https://www.spc.noaa.gov/exper/ma_archive/.

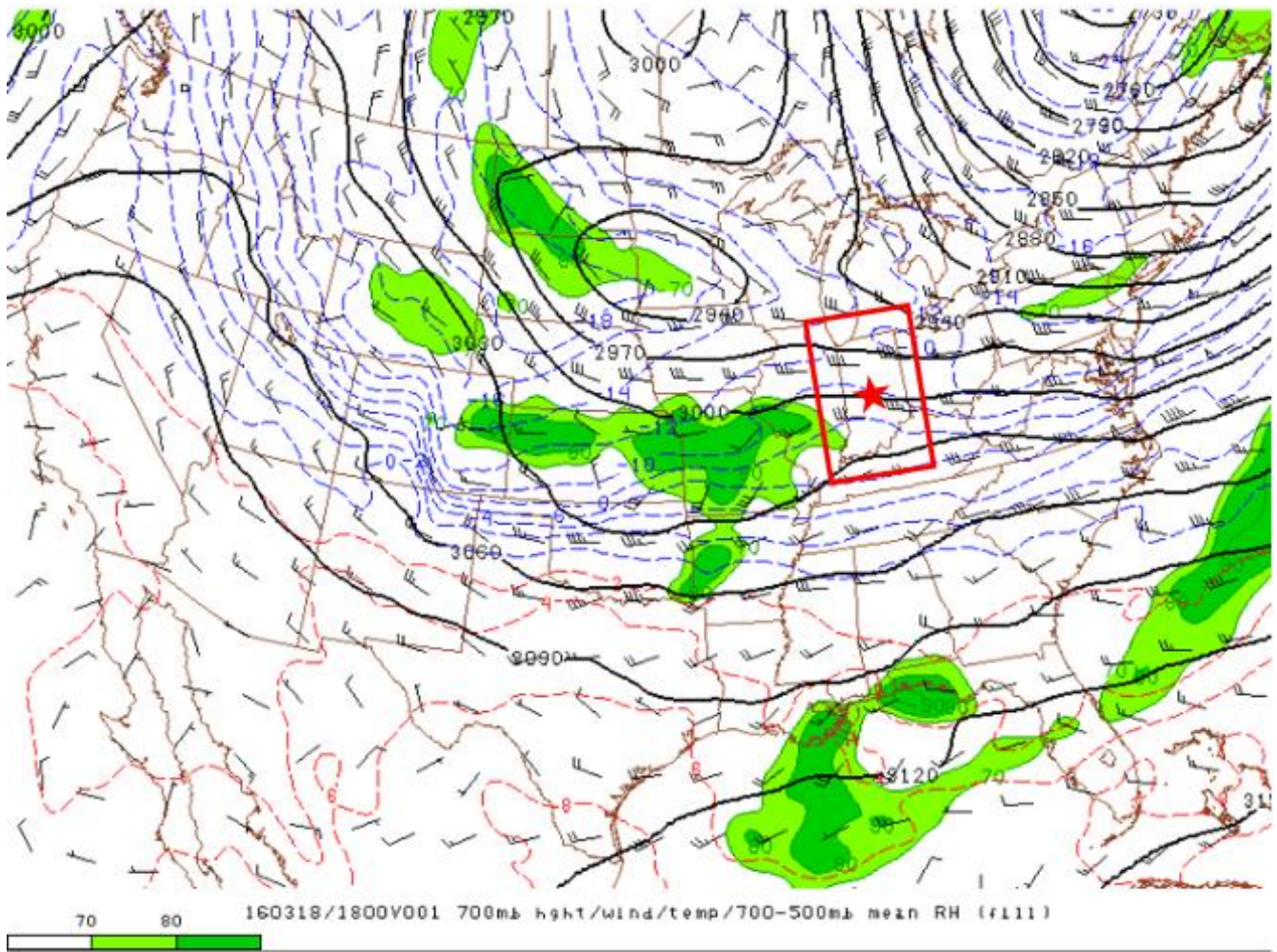


Figure S5.3. Weather map of mid-troposphere (3-5.5 km) relative humidity on the DBL case study day (18 March 2016) at 14:00 local time (EDT). Figure S5.3 shows moistening ahead of a shortwave trough. Indiana is outlined by a red box, and Indianapolis is indicated with a star. The dark green coloring shows relative humidity greater than 80%. This weather map supports observations of elevated H_2O_v mole fraction in the free troposphere during the fourth vertical profile (VP4) on DBL. Map source: https://www.spc.noaa.gov/exper/ma_archive/.

Section S6. Fractionation of water vapor in ice supersaturated conditions

H_2O_v undergoing deposition on ice crystals is impacted by equilibrium and kinetic fractionation. The kinetic fractionation factor is calculated via Galewsky (2015) eq. (S6.1):

$$\alpha_{ice,k} = \frac{S_i}{\alpha_e \frac{D}{D'} (S_i - 1) + 1}, \quad (\text{S6.1})$$

where S_i is saturation with respect to ice, expressed as a fraction. The equilibrium fractionation factor, α_e , is calculated for the temperature at the lifting condensation level (LCL) and is discussed in Methods 2.5. The ratio of the molecular diffusivity of the light to heavy isotopologue, $\frac{D}{D'}$, is 1.02849 for ^{18}O and 1.02512 for D (Merlivat, 1978).

The isotopic signature of an air parcel in ice supersaturated conditions (R_{S_i}) can be calculated according to eq. (S6.2):

$$R_{S_i} = R_o \left(\frac{H_2O_v}{H_2O_{v_o}} \right)^{\alpha_{ice,k} \alpha_e^{-1}} \quad (\text{S6.2})$$

R_o is the heavy to light isotopologue ratio ($\frac{HDO_v}{H_2O_v}$ or $\frac{H_2^{18}O_v}{H_2O_v}$) of the parcel prior to the ascent. The remaining fraction of H_2O_v left in the ascending parcel relative to initial conditions is given by $\frac{H_2O_v}{H_2O_{v_o}}$.

Figure S6 shows the STC VP d-excess observations along with Rayleigh vapor calculated from $\text{RH} = 100\%$ (Methods 2.5) and vapor in ice supersaturated conditions (eq. (S6.2)). To match the most negative d-excess value observed at the top of the INV on STC, a supersaturation (S_i) of 1.17 ($\text{RH}_i = 117\%$ in Fig. S6) was used but does not necessarily reflect reality for the temperature or altitude of the observations. The Rayleigh curve is presented for reference.

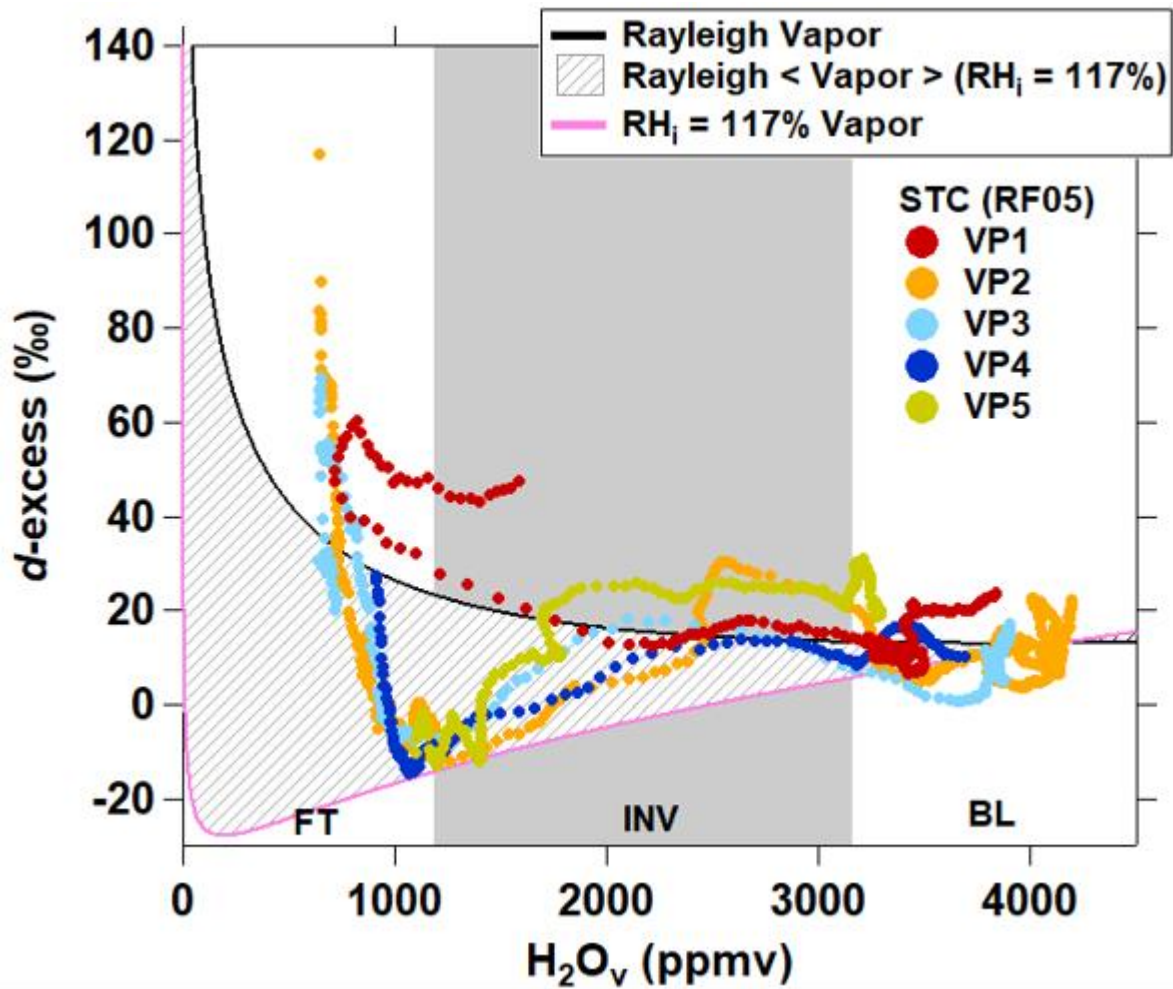


Figure S6: STC VP d-excess observations, Rayleigh vapor d-excess, and calculated d-excess of vapor in ice supersaturated (RH_i) conditions up to $RH_i = 117\%$. Ice supersaturated conditions were chosen merely to match the INV-FT interface d-excess observations, and do not necessarily reflect a realistic RH_i for the STC flight day. The region indicated by the slanted lines describes the Rayleigh-predicted d-excess values under conditions spanning 100% RH over liquid to 117% RH_i over ice.

Section S7. Indianapolis International Airport (KIND) temperature and dewpoint profiles preceding and during DBL observations

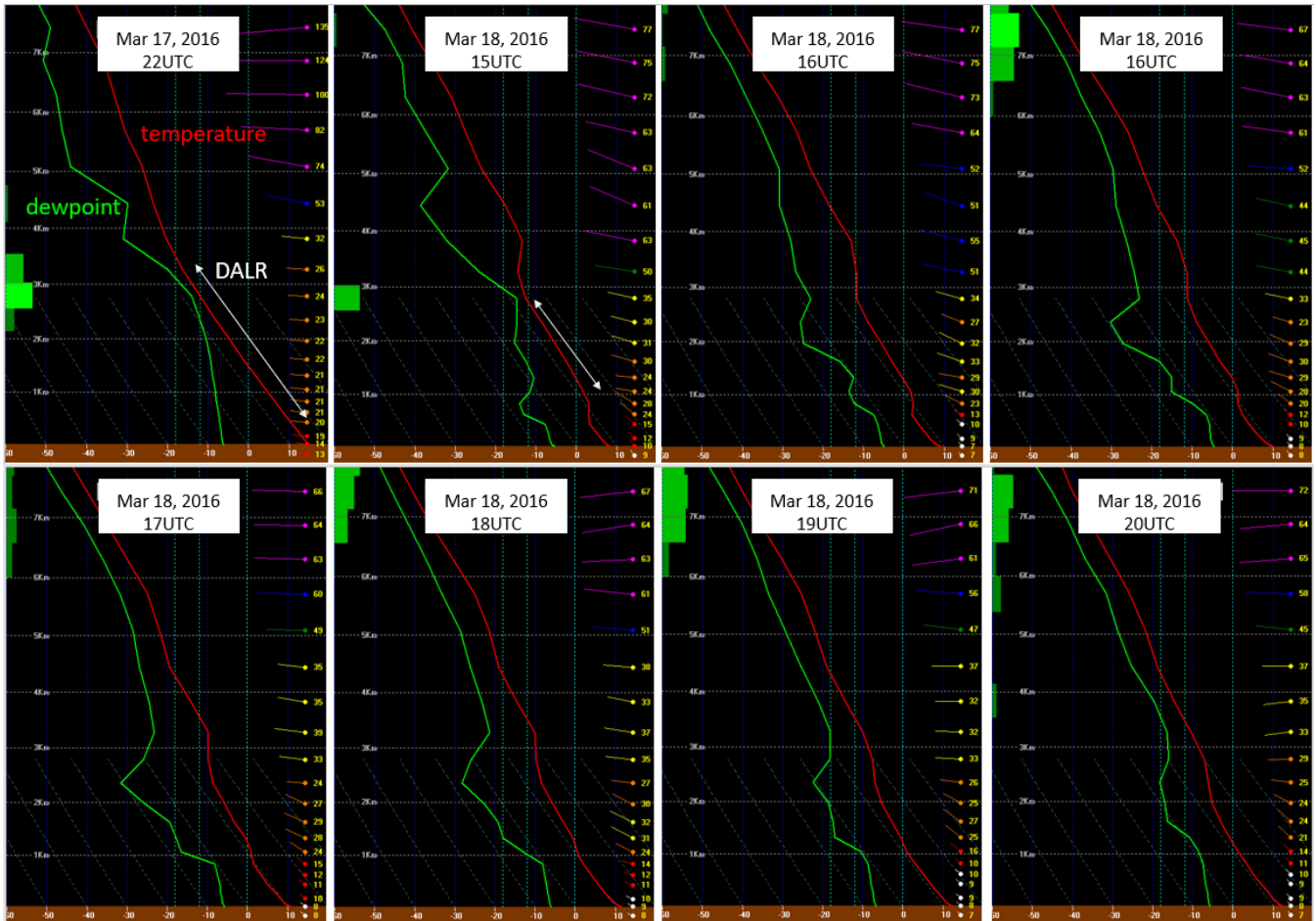


Figure S7. Rapid Refresh (RAP) Model ambient temperature and dewpoint profiles for the Indianapolis International Airport (KIND) from 22:00 EDT on 17 March 2018 (MAR17; Table 1) and 11:00 – 17:00 EDT on 18 March 2016 (MAR18-DBL; Table 1). The progression of figures shows a near dry adiabatic lapse rate (DALR; white line) persisted from 17 March 2018 into the afternoon of 18 March 2018. With time, the 17 March 2018 residual layer (with nearly a DALR) is incorporated into the 18 March 2018 boundary layer.